Journal of Sound and Vibration 333 (2014) 6258–6272

Contents lists available at ScienceDirect

Journal of Sound and Vibration

journal homepage: www.elsevier.com/locate/jsvi

Rotordynamic analysis using the Complex Transfer Matrix: An application to elastomer supports using the viscoelastic correspondence principle

Philip Varney*, Itzhak Green

Georgia Institute of Technology, Woodruff School of Mechanical Engineering, 801 Ferst Drive, Atlanta, GA 30332, United States

ARTICLE INFO

Article history:
Received 10 December 2013
Received in revised form
17 May 2014
Accepted 24 June 2014
Handling Editor: S. Ilanko
Available online 18 July 2014

ABSTRACT

Numerous methods are available to calculate rotordynamic whirl frequencies, including analytic methods, finite element analysis, and the transfer matrix method. The typical real-valued transfer matrix (RTM) suffers from several deficiencies, including lengthy computation times and the inability to distinguish forward and backward whirl. Though application of complex coordinates in rotordynamic analysis is not novel per se, specific advantages gained from using such coordinates in a transfer matrix analysis have yet to be elucidated. The present work employs a complex coordinate redefinition of the transfer matrix to obtain reduced forms of the elemental transfer matrices in inertial and rotating reference frames, including external stiffness and damping. Application of the complex-valued state variable redefinition results in a reduction of the 8×8 RTM to the 4×4 Complex Transfer Matrix (CTM). The CTM is advantageous in that it intrinsically separates forward and backward whirl, eases symbolic manipulation by halving the transfer matrices' dimension, and provides significant improvement in computation time. A symbolic analysis is performed on a simple overhung rotor to demonstrate the mathematical motivation for whirl frequency separation. The CTM's utility is further shown by analyzing a rotordynamic system supported by viscoelastic elastomer rings. Viscoelastic elastomer ring supports can provide significant damping while reducing the cost and complexity associated with conventional components such as squeeze film dampers. The stiffness and damping of a viscoelastic damper ring are determined herein as a function of whirl frequency using the viscoelastic correspondence principle and a constitutive fractional calculus viscoelasticity model. The CTM is then employed to obtain the characteristic equation, where the whirl frequency dependent stiffness and damping of the elastomer supports are included. The Campbell diagram is shown, demonstrating the CTM's ability to intrinsically separate synchronous whirl direction for a non-trivial rotordynamic system. Good agreement is found between the CTM results and previously obtained analytic and experimental results for the elastomer ring supported rotordynamic system.

1. Introduction

Determining rotor whirl frequencies (i.e., eigenvalues) is central to a comprehensive rotordynamic analysis. Whirl, defined as the rotor's bulk precession about its undeflected axis, is characterized by its direction relative to the shaft

* Corresponding author.
E-mail addresses: pvarney3@gatech.edu (P. Varney), itzhak.green@me.gatech.edu (I. Green).

http://dx.doi.org/10.1016/j.jsv.2014.06.036
0022-460X/

rotation. Forward whirl occurs in the direction of shaft rotation, while backward whirl occurs opposite the direction of shaft rotation [1] (as will be seen, a disadvantage of typical transfer matrix techniques is the inability to distinguish forward and backward whirl). Whirl frequencies are also categorized as synchronous or non-synchronous; synchronous whirl results when the whirl frequency coincides with the shaft speed [2]. Knowledge of the whirl frequencies and their direction is important for several reasons. First, changes in the whirl frequencies can elucidate changes in system properties, such as the support stiffness. Second, and more importantly, these free response parameters dictate the nature of the forced response. Imbalance is a forward synchronous excitation, resulting in resonant-like conditions when the shaft speed coincides with the forward synchronous whirl frequency (i.e., a rotor critical speed). In the same manner, resonant-like conditions arise when a backward synchronous whirl frequency coincides with the frequency of a backward excitation. Knowledge of a system's synchronous whirl frequencies and their directions is imperative to avoid undesirable operation near the critical speeds.

A multitude of analysis techniques can be applied to ascertain the whirl frequencies of rotordynamic systems. If closed-form equations of motion can be found, determining whirl frequencies amounts to finding the eigenvalues analytically as a function of shaft speed (the locus of whirl frequencies versus shaft speed is referred to as the Campbell diagram). Such an approach is often possible for Jeffcott rotors [1,3], modified Jeffcott rotors [3–5], simple overhung rotors [1,3], and simple cracked or asymmetric systems. Varney [6] compares the Campbell diagram of a notched overhung shaft to an overhung shaft displaying an open fatigue crack; the results are qualitatively corroborated by Lee [3] and Tondl [5].

The complexity of many rotordynamic systems necessitates approximation techniques; one commonly used method is finite element analysis. Nelson and McVaugh [7] develop a finite element for a rotating beam segment, including rotary inertia, gyroscopic effects, axial degrees of freedom, and linear external stiffness and damping. The derivation includes results for both rotating and inertial reference frames. A method for finding the inertial whirl frequencies is also described in their work. Nelson [8] extends this finite element to include Timoshenko beam theory; this element has enjoyed widespread use in many rotordynamic works, such as that by Darpe et al. [9]. Summaries of the finite element technique for whirl speed analysis are provided by Genta [1] and Rao [2].

The transfer matrix method is a discretization technique adept at quickly and accurately analyzing complex rotordynamic systems by seamlessly accounting for rotordynamic properties and phenomena such as support reactions (e.g., external bearing stiffness and damping), external forcing, and complicated geometry. Originally developed by Myklestad [10,11] and Prohl [12], the transfer matrix condenses elemental steady-state equations of motion into a single matrix relating the forces and displacements on either end of the element. Pestel and Leckie [13] provide a thorough discussion of the method, including numerous examples. Many works have not only applied but also improved the transfer matrix method. Notably, Lund and Orcutt [14] and Lund [15] modify the technique to estimate the critical speeds and stability regions of a flexible rotor supported on fluid film bearings. Murphy and Vance [16] provide an improved transfer matrix based on a reorganization of the calculation scheme. Lee and Green [17] develop the Complex Extended Transfer Matrix to account for external harmonic excitation. Choi and Mau [18] include gear stiffness and damping to calculate the critical speeds of a geared rotor system. Hsieh et al. [19,20] provide transfer matrices giving the coupling between lateral and torsional degrees of freedom, and model the rotor as having distributed mass. Several authors modify the transfer matrix to include asymmetric beam segments [6,20–22].

The transfer matrix has several notable advantages compared to finite element methods. First, the transfer matrix method is well-suited for symbolic manipulation; Varney and Green [23] use symbolic transfer matrices to find the stiffness matrix of an overhung rotor with a gaping fatigue crack. Second, the sequential multiplication of elemental transfer matrices is natural to rotordynamic systems. Finally, the transfer matrix method provides significant expediency in extracting the steady-state response without resorting to numeric integration. Yet, the finite element method still retains several advantages over the transfer matrix method. Importantly, finite element analysis allows for nonlinear effects to be included. For example, the nonlinear nature of a breathing crack would necessitate the use of finite element methods. Second, the robustness of finite element analysis easily allows for the inclusion of many rotordynamic components and configurations. Finally, the finite element analysis can provide the transient response of the rotor. Some effort has been made to incorporate these abilities into the transfer matrix method. For example, Liew et al. [24] provide an adaptation of the transfer matrix method to include nonlinearities and transient response by assembling differential equations of motion in a manner similar to finite element analysis.

Previous works employing the transfer matrix method (such as those discussed earlier) use real-valued coordinates. The 8×8 Real Transfer Matrix (RTM) analyzes rotor motion in orthogonal planes, and suffers from several deficiencies such as (1) increased computation times, (2) decreased eigenvalue accuracy due to the characteristic equation's high degree, and, most importantly, (3) the inability to distinguish forward and backward whirl. This work proposes a complex-valued state variable redefinition to obtain reduced 4×4 forms of the elemental transfer matrices, resulting in the Complex Transfer Matrix (CTM). Several advantages are gained from this novel redefinition of the transfer matrix state vector: increased computational efficiency, improved accuracy, and intrinsic separation of forward and backward whirl. Knowledge of whirl speed direction is important, as different excitations can excite both forward and backward whirl frequencies (for example, rotor–stator contact introduces forward and backward excitations [25–28]).

The application of complex coordinates in rotordynamics is not unique per se; complex coordinates have enjoyed widespread use in rotordynamics from the earliest developments in the field. Early texts by Tondl [5] and Dimentberg [29] apply complex coordinates in their analyses. Lee [3] and Genta [1] make extensive use of complex coordinates, most notably

for the analysis of analytically obtained equations of motion. In their works, both authors highlight the ability of complex coordinates to distinguish forward and backward whirl. In fact, Genta [1] suggests a complex coordinate transfer matrix for damped systems, though detailed results and interpretations are not provided. This representative summary of works employing complex coordinates is not encompassing; many other authors employ complex coordinates in their works.

This work's novelty lies not in the direct use of complex coordinates, but in their application to the transfer matrix method. In addition, a symbolic mathematical analysis detailing the reason for whirl speed separation is provided. A simple overhung rotor is used as an example to elucidate various benefits associated with the CTM. Additionally, the present work incorporates viscoelastic elastomer ring supports into a rotor model using the CTM. The support's stiffness and damping are found using the viscoelastic correspondence principle and a fractional calculus constitutive model, and incorporated into the transfer matrix for the first time. Details on the fractional calculus constitutive model are provided by Szumski and Green [30] and Smyth [31]. The support stiffness and damping are directly related to the storage and loss moduli of the elastomer, and as such display significant frequency dependency [31]. This frequency dependency is elegantly and directly incorporated into the transfer matrix using the viscoelastic correspondence principle, in a manner analogous to the approach used to couple the dynamics of a gas lubricated seal to the frequency-dependent properties of the lubricant film [32]. Such an approach allows the rotor's synchronous whirl frequencies to be determined directly rather than iteratively. The analytic results obtained herein are compared to analytic and experimental results obtained by Scholz [33] and Liebich et al. [34].

2. The Real Transfer Matrix (RTM)

The foundation of the transfer matrix method is free body diagrams of system components. The free body diagram of a lumped mass in the *xz* and *yz* planes is shown in Fig. 1; the figure shown is valid for an inertial or rotating reference frame, though the specific definitions of the variables shown may change depending on the frame. The lumped mass m_i has polar and transverse mass moments of inertia of I_{p_i} and I_{t_i}, respectively. The lateral displacements are u_x and u_y, while the rotations are θ_x and θ_y. Internal shear and moment reactions are generated on the left (L) and right (R) sides of the element, and are designated V and M, respectively.

External stiffness and damping forces are included (F_j^S and F_j^C, respectively), where the subscript indicates the appropriate direction. The current work leaves the stiffness and damping in a general form, whereas [17] includes only angular stiffness and damping due to a mechanical face seal, and Green and Casey [35] include only internal damping in a rotating frame. Such a generalization permits the inclusion of a variety of rotordynamic triboelements such as fluid film bearings, mechanical face seals, and, as will be demonstrated, viscoelastic elastomer supports.

The lateral and angular displacements, internal shear, and internal bending moments form the state vector:

$$\mathbf{S}_i = \{u_x \;\; \theta_y \;\; M_y \;\; -V_x \;\; -u_y \;\; \theta_x \;\; M_x \;\; V_y\}^T, \tag{1}$$

where all entries are real-valued quantities. The state vector is the backbone of the transfer matrix method, as the elemental matrices transfer the state vector across an element. Such elemental transfer matrices incorporate the inertial and/or elastic properties of the physical component. Inertial effects are incorporated into a point matrix and elastic effects are encapsulated in the field matrix. These matrices are derived herein for both inertial and rotating reference frames.

2.1. Inertial frame

The forces on a point element are due to internal shear, internal bending, and external stiffness and damping, as shown in Fig. 1. The external stiffness and damping forces are, respectively,

$$\begin{Bmatrix} F_x^S \\ F_y^S \end{Bmatrix} = -\begin{bmatrix} k_{xx} & k_{xy} \\ k_{yx} & k_{yy} \end{bmatrix} \begin{Bmatrix} u_x \\ u_y \end{Bmatrix} \tag{2}$$

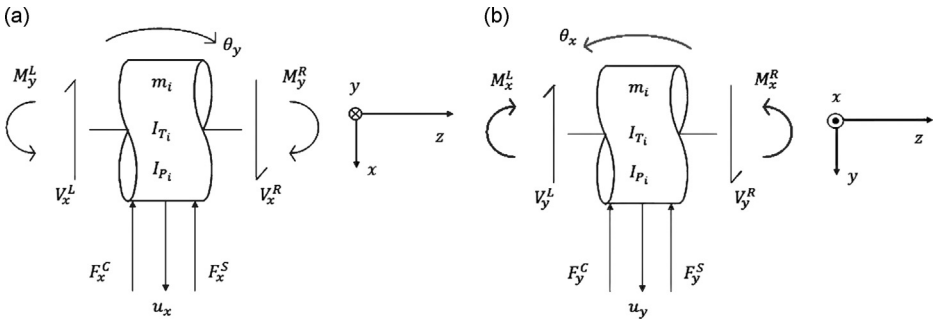

Fig. 1. Point element formulation. (a) Bending in the *xz* plane; (b) bending in the *yz* plane.

$$\begin{Bmatrix} F_x^C \\ F_y^C \end{Bmatrix} = -\begin{bmatrix} d_{xx} & d_{xy} \\ d_{yx} & d_{yy} \end{bmatrix} \begin{Bmatrix} \dot{u}_x \\ \dot{u}_y \end{Bmatrix}. \tag{3}$$

Equating the dynamic and applied forces on point element i provides two equations of motion:

$$m_i \ddot{u}_x = V_x^R - V_x^L - F_x^C - F_x^S \tag{4}$$

$$m_i \ddot{u}_y = V_y^R - V_y^L - F_y^C - F_y^S. \tag{5}$$

Expressing the angular momentum about the rotor's center of mass decouples the linear and angular degrees of freedom. Equating dynamic and applied moments gives the equations governing the angular motion (see [6] for details):

$$I_{t_i} \ddot{\theta}_x + I_{p_i} n \dot{\theta}_y = M_x^R - M_x^L \tag{6}$$

$$I_{t_i} \ddot{\theta}_y - I_{p_i} n \dot{\theta}_x = M_y^R - M_y^L. \tag{7}$$

Kinematic continuity across the point element gives the following relations:

$$u_x^R = u_x^L \tag{8}$$

$$u_y^R = u_y^L \tag{9}$$

$$\theta_x^R = \theta_x^L \tag{10}$$

$$\theta_y^R = \theta_y^L. \tag{11}$$

The response of each state vector variable occurs at the whirl frequency p. Assuming a solution of the form $\exp(\mathrm{j}pt)$ for every variable gives the following relations, written such that the element's right-side state vector variables are a function of those on the left:

$$u_x^R = u_x^L$$

$$\theta_y^R = \theta_y^L$$

$$M_y^R = -I_{t_i} p^2 \theta_y^L - \mathrm{j}\, I_{p_i} p n \theta_x^L + M_y^L$$

$$V_x^R = (-m_i p^2 + \mathrm{j}\, d_{xx} p + k_{xx}) u_x^L + (\mathrm{j}\, d_{xy} p + k_{xy}) u_y^L + V_x^L$$

$$u_y^R = u_y^L$$

$$\theta_x^R = \theta_x^L$$

$$M_x^R = -I_{t_i} p^2 \theta_x^L + \mathrm{j}\, I_{p_i} p n \theta_y^L + M_x^L$$

$$V_y^R = (-m_i p^2 + \mathrm{j}\, d_{yy} p + k_{yy}) u_y^L + (\mathrm{j}\, d_{yx} p + k_{yx}) u_x^L + V_y^L. \tag{12}$$

Placing these equations into matrix form provides the point matrix $\mathbf{P}_i$ for the ith point element in an inertial frame:

$$\mathbf{P}_i = \begin{bmatrix} 1 & 0 & 0 & 0 & 0 & 0 & 0 & 0 \\ 0 & 1 & 0 & 0 & 0 & 0 & 0 & 0 \\ 0 & -I_{t_i} p^2 & 1 & 0 & 0 & -\mathrm{j}\, I_{p_i} n p & 0 & 0 \\ m_i p^2 - \mathrm{j}\, d_{xx} p - k_{xx} & 0 & 0 & 1 & \mathrm{j}\, d_{xy} p + k_{xy} & 0 & 0 & 0 \\ 0 & 0 & 0 & 0 & 1 & 0 & 0 & 0 \\ 0 & 0 & 0 & 0 & 0 & 1 & 0 & 0 \\ 0 & \mathrm{j}\, I_{p_i} n p & 0 & 0 & 0 & -I_{t_i} p^2 & 1 & 0 \\ \mathrm{j}\, d_{yx} p + k_{yx} & 0 & 0 & 0 & m_i p^2 - \mathrm{j}\, d_{yy} p - k_{yy} & 0 & 0 & 1 \end{bmatrix}. \tag{13}$$

The field matrix for the ith beam section is found in a similar manner using the Euler–Bernoulli beam theory (see Lee and Green [17] for details):

$$\mathbf{F}_i = \begin{bmatrix} 1 & L & \frac{L^2}{2EI} & \frac{L^3}{6EI} & 0 & 0 & 0 & 0 \\ 0 & 1 & \frac{L}{EI} & \frac{L^2}{2EI} & 0 & 0 & 0 & 0 \\ 0 & 0 & 1 & L & 0 & 0 & 0 & 0 \\ 0 & 0 & 0 & 1 & 0 & 0 & 0 & 0 \\ 0 & 0 & 0 & 0 & 1 & L & \frac{L^2}{2EI} & \frac{L^3}{6EI} \\ 0 & 0 & 0 & 0 & 0 & 1 & \frac{L}{EI} & \frac{L^2}{2EI} \\ 0 & 0 & 0 & 0 & 0 & 0 & 1 & L \\ 0 & 0 & 0 & 0 & 0 & 0 & 0 & 1 \end{bmatrix}, \tag{14}$$

where the element length is L, the modulus of elasticity is E, and the cross-sectional area moment of inertia of the shaft is I. The procedure assumes a symmetric beam element with constant cross section.

2.2. Rotating frame

An analogous procedure gives the rotating frame point matrix, though external stiffness and damping forces are excluded (these can be included using the Complex Extended Transfer Matrix [17]). The acceleration and angular momentum in the rotating frame are derived by Varney [6] and Green and Casey [35]. In the rotating frame, the response occurs at the relative whirl frequency p_r. The rotating-frame point matrix is

$$\mathbf{P}_i = \begin{bmatrix} 1 & 0 & 0 & 0 & 0 & 0 & 0 & 0 \\ 0 & 1 & 0 & 0 & 0 & 0 & 0 & 0 \\ 0 & (I_{p_i} - I_{t_i})n^2 - I_{t_i}p_r^2 & 1 & 0 & 0 & \mathrm{j}(2I_{t_i} - I_{p_i})np_r & 0 & 0 \\ m_i(p_r^2 + n^2) & 0 & 0 & 1 & 2\mathrm{j}\, m_i np_r & 0 & 0 & 0 \\ 0 & 0 & 0 & 0 & 1 & 0 & 0 & 0 \\ 0 & 0 & 0 & 0 & 0 & 1 & 0 & 0 \\ 0 & -\mathrm{j}(2I_{t_i} - I_{p_i})np_r & 0 & 0 & 0 & (I_{p_i} - I_{t_i})n^2 - I_{t_i}p_r^2 & 1 & 0 \\ -2\mathrm{j}\, m_i np_r & 0 & 0 & 0 & m_i(p_r^2 + n^2) & 0 & 0 & 1 \end{bmatrix}. \tag{15}$$

The field matrix is unchanged by the rotating frame, and is still therefore given by Eq. (14).

3. The Complex Transfer Matrix (CTM)

A complex redefinition of the state vector quantities is proposed to reduce the 8×8 RTM to the 4×4 Complex Transfer Matrix (CTM). As will be demonstrated, the new formulation results in several advantages: increased computational efficiency, improved accuracy, and intrinsic separation of forward and backward whirl. The basis of the CTM is a complex coordinate redefinition of the state vector elements, which is valid for both the inertial and rotating reference frames:

$$u = u_x + \mathrm{j}\, u_y$$

$$\theta = \theta_x + \mathrm{j}\, \theta_y$$

$$M = M_x + \mathrm{j}\, M_y$$

$$V = V_x + \mathrm{j}\, V_y. \tag{16}$$

This coordinate redefinition reduces the state vector in Eq. (1) to

$$\mathbf{S}_i = \{-u \;\; \theta \;\; M \;\; V\}^T. \tag{17}$$

The point and field matrices are reformulated using this complex coordinate redefinition for an inertial and rotating frame.

3.1. Inertial frame

The complex coordinate redefinition in Eq. (16) condenses the inertial frame point matrix, Eq. (13), into

$$(\mathbf{P}_i)_{4\times4} = \begin{bmatrix} 1 & 0 & 0 & 0 \\ 0 & 1 & 0 & 0 \\ 0 & -I_{t_i}p^2 + I_{p_i}np & 1 & 0 \\ m_i p^2 + W_{ext} & 0 & 0 & 1 \end{bmatrix}, \tag{18}$$

where W_{ext} includes the effects of external stiffness and damping:

$$W_{ext} = -(d_{xx} + \mathrm{j}\, d_{xy})p - (k_{xx} - \mathrm{j}\, k_{xy}). \tag{19}$$

It is imperative to note that the reduction of external stiffness and damping depends on the following assumptions: $k_{xx} = k_{yy}$, $k_{yx} = -k_{xy}$, $d_{xx} = d_{yy}$, and $d_{yx} = -d_{xy}$. If these conditions on the stiffness and damping coefficients are not met, the values can be averaged to obtain an approximation.

The complex coordinate redefinition results in the following 4×4 complex field matrix for symmetric beam element i:

$$\mathbf{F}_i = \begin{bmatrix} 1 & \mathrm{j}L & \mathrm{j}\dfrac{L^2}{2EI} & \dfrac{L^3}{6EI} \\ 0 & 1 & \dfrac{L}{EI} & -\mathrm{j}\dfrac{L^2}{2EI} \\ 0 & 0 & 1 & -\mathrm{j}L \\ 0 & 0 & 0 & 1 \end{bmatrix}, \tag{20}$$

which is valid only for beams with a symmetric cross-section.

This method is designated the CTM due to the nature of the transformation and the nature of the matrix elements themselves. The 4×4 field matrix in Eq. (20) is inherently complex, while the 4×4 point matrix in Eq. (18) contains complex terms if the cross-coupling coefficients d_{xy} and k_{xy} are non-zero.

3.2. Rotating frame

Application of Eq. (16) to the rotating frame equations of motion results in the following 4×4 point matrix for mass i:

$$\mathbf{P}_i = \begin{bmatrix} 1 & 0 & 0 & 0 \\ 0 & 1 & 0 & 0 \\ 0 & I_{p_i}n(p_r + n) - I_{t_i}(p_r + n)^2 & 1 & 0 \\ m_i(p_r + n)^2 & 0 & 0 & 1 \end{bmatrix}. \tag{21}$$

The complex field matrix $\mathbf{F}$, Eq. (20), is valid regardless of whether the frame is inertial or rotating.

It is well known [2,3,35–37] that rotating-frame eigenvalues are shifted from the absolute eigenvalues by the shaft speed of the system according to

$$p = p_r + n, \tag{22}$$

where p is the absolute eigenvalue, p_r is the relative eigenvalue, and n is the shaft speed. In fact, Eq. (21) reduces to Eq. (18) when p is replaced by $p_r + n$.

4. Simple overhung system: a comparison

A simple overhung rotor is analyzed using the RTM and the CTM to (a) demonstrate the method for obtaining whirl frequencies using the transfer matrix, (b) examine symbolically and numerically the advantages of the CTM, and (c) explain mathematically why the CTM distinguishes forward and backward whirl. A real, experimental rotordynamic system will subsequently be analyzed using the CTM. The overhung rotor is shown in Fig. 2, where the diameter of the uniform, massless shaft is d and the length is L. The boundary conditions are such that the left end is cantilevered (i.e., no lateral or

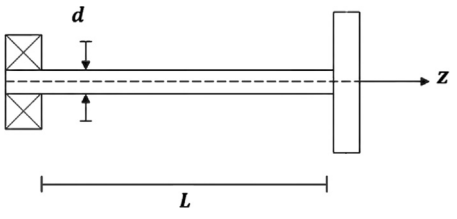

Fig. 2. Overhung rotordynamic system.

angular displacements) while the right end is free (i.e., no internal shear or moment reactions). The rotor consists of a single lumped mass, with mass m and polar and transverse mass moments of inertia of I_p and I_t, respectively. The elastic modulus of the shaft is E, and the diameter of the shaft is used to calculate the area moment of inertia, I. External stiffness and damping are not included in this analysis, without any loss of generality.

The boundary conditions at the support (shown using the 8×8 RTM) are

$$\mathbf{S}_0 = \{0\ \ 0\ \ M_y\ \ -V_x\ \ 0\ \ 0\ \ M_x\ \ V_y\}^T, \tag{23}$$

while those at the free end (the right end of the lumped mass) are

$$\mathbf{S}_1^R = \{u_x\ \ \theta_y\ \ 0\ \ 0\ \ -u_y\ \ \theta_x\ \ 0\ \ 0\}^T. \tag{24}$$

The field matrix of the massless beam segment updates $\mathbf{S}_0$ from the support to the left end of the lumped mass according to:

$$\mathbf{S}_1^L = \mathbf{F}\,\mathbf{S}_0. \tag{25}$$

In a similar manner, the state vector at the free end is found by updating $\mathbf{S}_1^L$ across the point element:

$$\mathbf{S}_1^R = \mathbf{P}\,\mathbf{S}_1^L. \tag{26}$$

Combining Eqs. (25) and (26) by eliminating the intermediate state vector gives a relationship between the boundary conditions:

$$\mathbf{S}_1^R = \mathbf{U}\,\mathbf{S}_0, \tag{27}$$

where the overall transfer matrix $\mathbf{U}$ is

$$\mathbf{U} = \mathbf{P}\,\mathbf{F}. \tag{28}$$

No specification has been made as to whether the frame is inertial or rotating; this generalization will be removed shortly. An eigenvalue problem is obtained from Eq. (27) by extracting out the rows which are equal to zero, while several columns in $\mathbf{U}$ are eliminated due to multiplication by zero. The determinant of this submatrix provides the characteristic equation of the system, which is a polynomial in the whirl frequency p. The coefficients of this polynomial are functions of the shaft speed n and the physical parameters of the system.

4.1. Symbolic analysis

The characteristic equation is found as a function of the shaft speed n, the absolute whirl frequency p, and the physical parameters of the system. Using the inertial frame RTM, the characteristic equation for the generally non-synchronous, undamped system is

$$Q_R(p) = a_8p^8 + a_6p^6 + a_4p^4 + a_2p^2 + 1 = 0. \tag{29}$$

The polynomial coefficients are evaluated symbolically and summarized in Table 1 for the undamped overhung rotor, noting that inclusion of damping generates odd powers of p in the characteristic equation. The constants A, B, and C are functions only of the physical parameters, and not of the shaft speed n:

$$A = \frac{I_t m L^2 (mL^5 + 3I_tL^3)}{18E^3I^3} \tag{30}$$

$$B = \frac{L^2(9I_t^2 + 7.5I_tmL^2 + m^2L^4)}{9E^2I^2} \tag{31}$$

Table 1
General non-synchronous characteristic equation coefficients in an inertial frame.

RTM	Coefficient	CTM	Coefficient
a_8	$\frac{I_t^2L^8m^2}{144E^4I^4}$	b_4	$\frac{I_tmL^4}{12E^2I^2}$
a_6	$A-\frac{I_p^2m^2L^8}{144E^4I^4}n^2$	b_3	$\frac{-I_pmL^4}{12E^2I^2}n$
a_4	$B+\frac{I_p^2mL^5}{6E^3I^3}n^2$	b_2	$\frac{-mL^3-3I_tL}{3EI}$
a_2	$C-\frac{I_p^2L^2}{E^2I^2}n^2$	b_1	$\frac{I_pL}{EI}n$

$$C = \frac{2L(mL^2 + 3I_t)}{3EI}. \tag{32}$$

It is clear from Table 1 that the shaft speed n appears in the RTM characteristic equation only in even powers; the same eigenvalues p are obtained regardless of whether n is positive (forward) or negative (backward). Thus, the RTM is incapable of distinguishing forward and backward whirl. The same ambiguity persists for a general system composed of many point masses and beam segments, with any combination of boundary conditions. An analogous rotating frame analysis is provided by Varney [6].

In comparison, the CTM generates the following generally non-synchronous characteristic equation:

$$Q_C(p) = b_4 p^4 + b_3 p^3 + b_2 p^2 + b_1 p + 1 = 0. \tag{33}$$

The coefficients of this polynomial for the simple overhung system are given symbolically in Table 1. In this case, it is clear that different whirl frequencies are obtained when n is either positive or negative. This unique trait of the CTM precipitates separation of forward and backward whirl. The comparative complexity of the terms in Table 1 also indicates another unique advantage of the CTM over the RTM: the ease of symbolic manipulation.

The synchronous whirl characteristic equations provide further insight into the CTM's unique separation capability. The forward and backward synchronous whirl characteristic equations obtained using the CTM are, respectively:

$$\frac{mL^4(I_t - I_p)}{12E^2I^2} p^4 + \frac{L(3I_p - 3I_t - mL^2)}{3EI} p^2 + 1 = 0 \tag{34}$$

and

$$\frac{mL^4(I_t + I_p)}{12E^2I^2} p^4 - \frac{L(3I_p + 3I_t + mL^2)}{3EI} p^2 + 1 = 0. \tag{35}$$

However, the characteristic equations found using the RTM are identical for forward and backward synchronous whirl. Distinction of forward and backward synchronous whirl is therefore impossible without further analysis. Moreover, these identical characteristic equations are merely a product of the characteristic equations found using the CTM for forward and backward synchronous whirl (i.e., the product of Eqs. (34) and (35)).

For each point matrix included in the overall transfer matrix, the order of the characteristic equation is incremented by either four (CTM) or eight (RTM). Therefore, for N point elements, the order of the characteristic equation is either $4N$ (CTM) or $8N$ (RTM). For systems with many point elements, the use of the RTM generates a characteristic equation of prohibitively high order. Hence, one advantage of the CTM is clear: the order of the characteristic equation is reduced by a factor of 2. The decrease in the order of the characteristic equation results in a significant decrease in computation time in addition to increased accuracy of the roots.

4.2. Numeric analysis

The RTM and CTM are used to analyze the simple system shown in Fig. 2. The analysis is performed in the inertial reference frame; a similar analysis in the rotating frame, though not given here for brevity, is provided by Varney [6]. The diameter of the circular cross-section overhung shaft is d, with elastic modulus E and cross-sectional area moment of inertia I. The shaft of length L is assumed to be massless compared to the rotor. The parameters of the system are summarized in Table 2. These parameters are chosen so that the majority of the whirl speeds are relatively close in magnitude, so as to best demonstrate the differences between the RTM and CTM methods. Campbell diagrams are generated using the RTM (Fig. 3a) and the CTM (Fig. 3b).

The generally non-synchronous whirl frequencies are found via the overall transfer matrix of the simple overhung system, Eq. (28). Application of boundary conditions reduces the overall transfer matrix to the corresponding eigenvalue problem, the roots of which are the generally non-synchronous whirl speeds (Eqs. (29) and (33) are found from the eigenvalue problem, giving the whirl frequencies for the RTM and CTM, respectively). The synchronous forward whirl frequencies are found by repeating the procedure with the condition $n = p$, while the backward synchronous whirl frequencies are found with $n = -p$. Equivalently, the forward and backward synchronous whirl frequencies are seen on the Campbell diagram where a line of slope 1 and -1 intersects the locus of whirl frequencies, respectively. It is clear from

Table 2
Parameters of the example system.

m	91.9 kg
I_t	1.436 kg m^2
I_p	0.718 kg m^2
E	206.9 GPa
L	0.2 m
d	0.05 m

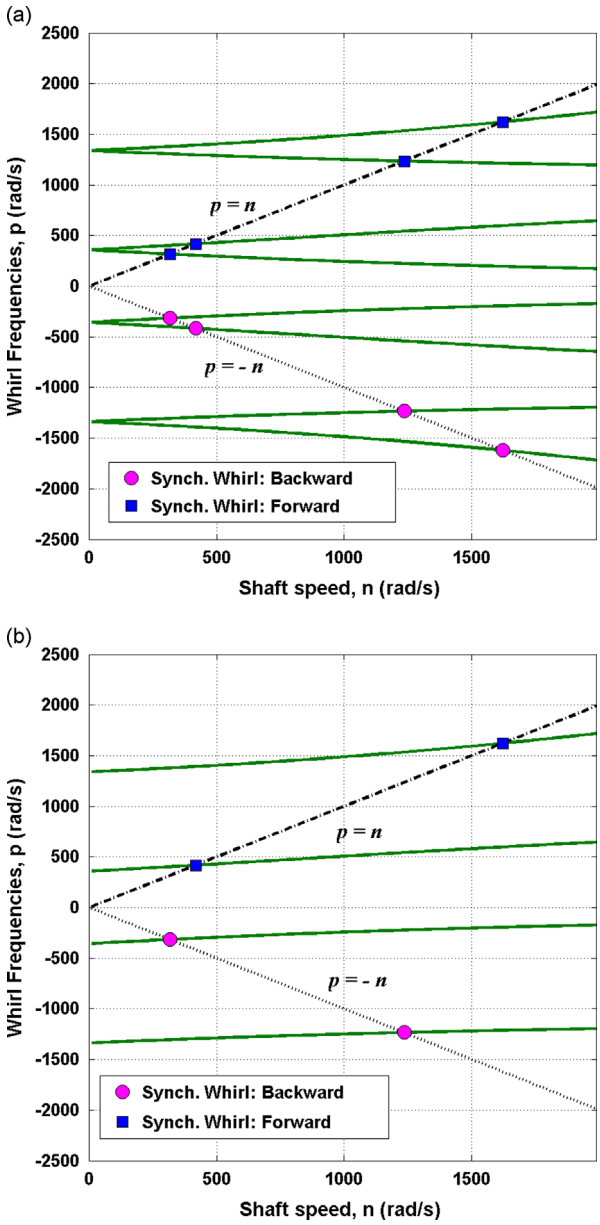

Fig. 3. Inertial frame comparison of the RTM and CTM for a simple overhung system. (a) RTM; (b) CTM.

Fig. 3a that the RTM is incapable of separating forward and backward whirl; each whirl speed, both synchronous and non-synchronous, is mirrored across the horizontal shaft speed axis. The ability of the CTM to distinguish these frequencies is seen in Fig. 3b, as each synchronous whirl speed is unique.

5. Elastomer ring dampers

The utility of the CTM is demonstrated via application to a non-trivial rotordynamic system: a two-disk rotor supported on viscoelastic elastomer rings. Analytic results generated herein are compared to analytic and experimental results provided by Scholz [33] and Liebich et al. [34]. The support stiffness and damping depend on the elastomer's storage and loss moduli; these moduli are determined experimentally by Scholz [33]. The experimental data is fit using a 1/2 exponent fractional calculus constitutive model, where the resulting analytic model is incorporated directly into the transfer matrix using the viscoelastic correspondence principle.

5.1. Elastomer stiffness and damping

External bearing damping is frequently necessitated in rotating machinery to alleviate undesirable machine vibration. Squeeze film dampers (SFD), which dissipate energy through viscous fluid displacement, have often been used towards this purpose; these components are not only complex but also costly. An alternative to the SFD is discussed by Scholz [33] and Liebich et al. [34]: the elastomer ring damper (ERD). The ERD provides external stiffness and damping by exploiting viscoelastic material properties.

The frequency-dependent complex modulus of the viscoelastic elastomer, E^*, is expressed in the frequency domain as [32]

$$E^*(p) = E'(p) + \mathrm{j}E''(p), \tag{36}$$

where the storage and loss moduli are E' and E'', respectively. Furthermore, the loss factor η is defined as the ratio of these quantities: $\eta = E'/E''$. These material properties were measured as a function of frequency by Scholz [33] and Liebich et al. [34] for HNBR-60 rubber. To compensate for the narrow range of permissible frequency measurements, the elastomer properties were instead measured at several temperatures. These measurements were concatenated into a master curve at a single reference temperature ($T_o = -15\ ^\circ\mathrm{C}$) using the temperature-frequency shift property of viscoelastic materials [38]:

$$\log(\alpha_T) = \log(f) - \log(f_o) \tag{37}$$

where α_T is the temperature shift parameter, f_o is a reference frequency, and f is the frequency of interest. The temperature shift parameter α_T is a material property dependent on the reference temperature T_o and the shifted temperature T_s. The temperature–frequency shift principle states that a change in operating temperature is equivalent to a shift in operating frequency at the reference temperature. The experimental data is fit in the frequency domain using a constitutive fractional calculus model with exponent 1/2 [30,31], such that the storage and loss moduli are obtained as analytic functions of frequency, p:

$$E'(p) = E_o + E_1\left(\frac{(\sqrt{2p}/2)\mu_1 + p}{\mu_1^2 + \mu_1\sqrt{2p} + p}\right) \tag{38}$$

$$E''(p) = E_1\left(\frac{(\sqrt{2p}/2)\mu_1}{\mu_1^2 + \mu_1\sqrt{2p} + p}\right). \tag{39}$$

The constitutive model parameters E_o, E_1, and μ_1 obtained through fitting the experimental data are $E_o = 7.5$ MPa, $E_1 = 2135.2$ MPa, $\mu_1 = 52.7\ \mathrm{s}^{-0.5}$. The experimental and analytic storage modulus $E'(p)$ and loss factor $\eta(p)$ are shown in Fig. 4.

The ERD geometry is shown in Fig. 5a, where the ring's mean diameter, width, and height are D_m, b, and h, respectively. The elastomer is sandwiched between two concentric steel rings, as designated in the figure. A form factor influencing the stiffness of the ring is given by Liebich et al. [34] to be

$$k_L = \frac{1}{6}\beta\left(5 + \beta^2\right) \tag{40}$$

where β is the ratio b/h. The stiffness k and damping c for N elastomer rings in parallel is given [33,34] as a function of frequency p:

$$k(p) = ND_m\pi k_L E'(p) \tag{41}$$

$$c(p) = k(p)\eta(p) \tag{42}$$

The elastomer ring's stiffness and damping are combined to give a complex stiffness, $z(p)$, using the viscoelastic correspondence principle [32]:

$$z(p) = k(p) + \mathrm{j}c(p) \tag{43}$$

5.2. Transfer matrix analysis

The experimental rotordynamic test rig described by Scholz [33] and Liebich et al. [34] is shown in Fig. 5b, where the rotor is supported externally such that there is no internal shear or moments at the boundaries. The relevant parameters are provided in Table 3, and the temperature of the elastomer is assumed to be the temperature at which experiments were performed, 25 °C (leading to a shift factor of $\alpha_T = 10^{-8}$ [33]). The shaft is divided such that the three segments from left to right are of lengths 220 mm, 260 mm, and 220 mm.

The steel shaft has density $\rho = 7950\ \mathrm{kg/m^3}$ and an elastic modulus of 206 GPa. One-third of the shaft's mass is split between the rotors, according to a typical approximation for discretizing continuous systems. The rotor's polar and transverse mass moments of inertia are found assuming the rotor to be a full disk. Eqs. (13) and (14) give the point and field matrices in the inertial reference frame for the RTM, while Eqs. (18) and (20) give the same matrices using the CTM.

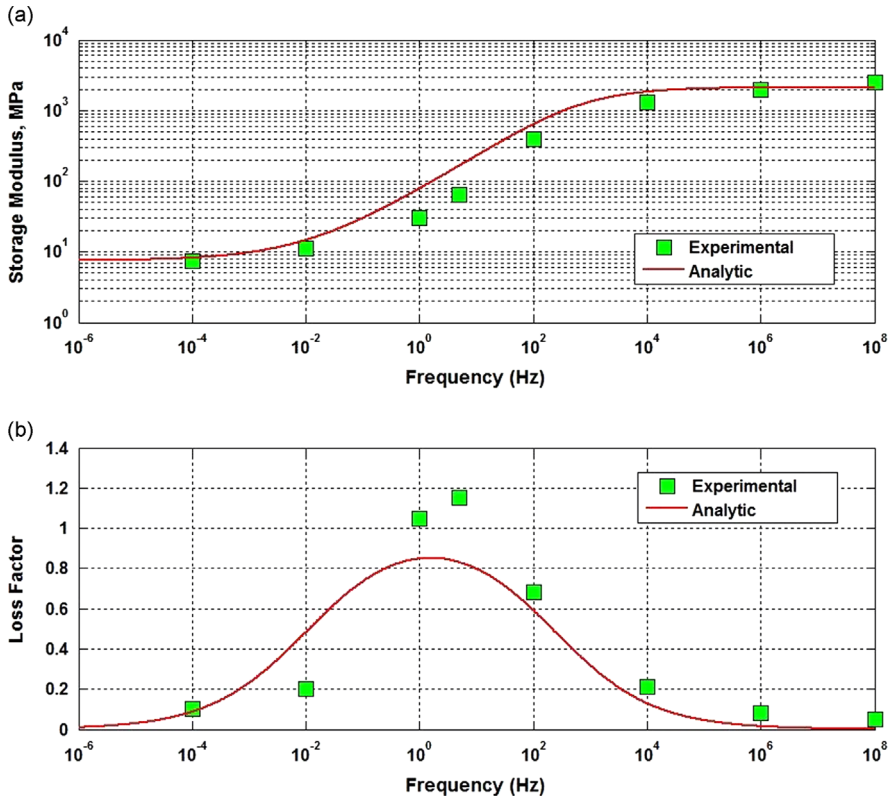

Fig. 4. Viscoelastic properties of HNBR-60 at $T_o = -15$ °C (experimental results according to Scholz [33]). (a) Storage modulus; (b) loss factor.

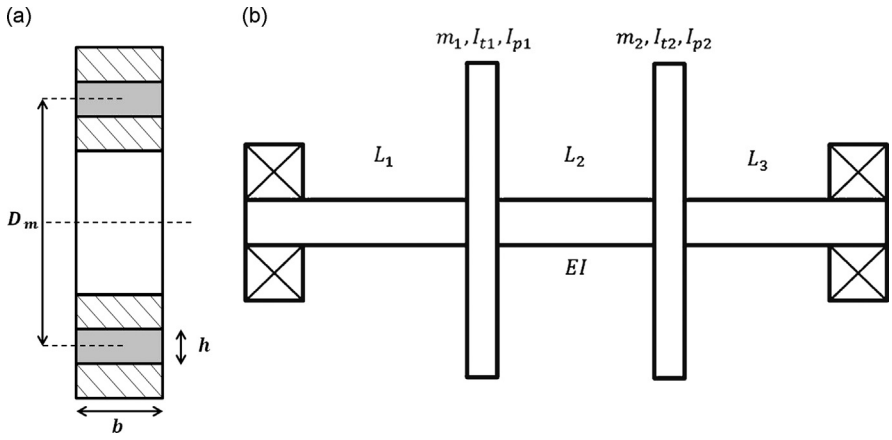

Fig. 5. Rotor and elastomer ring geometries, according to Scholz [33]. (a) Ring geometry; (b) rotordynamic system.

Table 3
Rotordynamic and elastomer ring parameters.

Rotor properties		**Elastomer ring properties**	
Shaft diameter, d	25 mm	Bearing diameter, D_m	68 mm
Rotor masses, m_1, m_2	4.8 kg	Bearing width, b	12 mm
Rotor radius, R	70 mm	Bearing height, h	6 mm
Rotor length, L	700 mm	Number of rings, N	1
Rotor thickness, t	30 mm		

The transfer matrix for an elastomer ring support is that of a point matrix with zero mass, and will be distinguished from a point matrix with inertia by the symbol **B**. The external stiffness and damping are provided by Eqs. (41) and (42), respectively. The bearing matrix, **B**, using the RTM and assuming no mass at the bearing, is

$$\mathbf{B} = \begin{bmatrix} 1 & 0 & 0 & 0 & 0 & 0 & 0 & 0 \\ 0 & 1 & 0 & 0 & 0 & 0 & 0 & 0 \\ 0 & 0 & 1 & 0 & 0 & 0 & 0 & 0 \\ -z(p) & 0 & 0 & 1 & 0 & 0 & 0 & 0 \\ 0 & 0 & 0 & 0 & 1 & 0 & 0 & 0 \\ 0 & 0 & 0 & 0 & 0 & 1 & 0 & 0 \\ 0 & 0 & 0 & 0 & 0 & 0 & 1 & 0 \\ 0 & 0 & 0 & 0 & -z(p) & 0 & 0 & 1 \end{bmatrix} \tag{44}$$

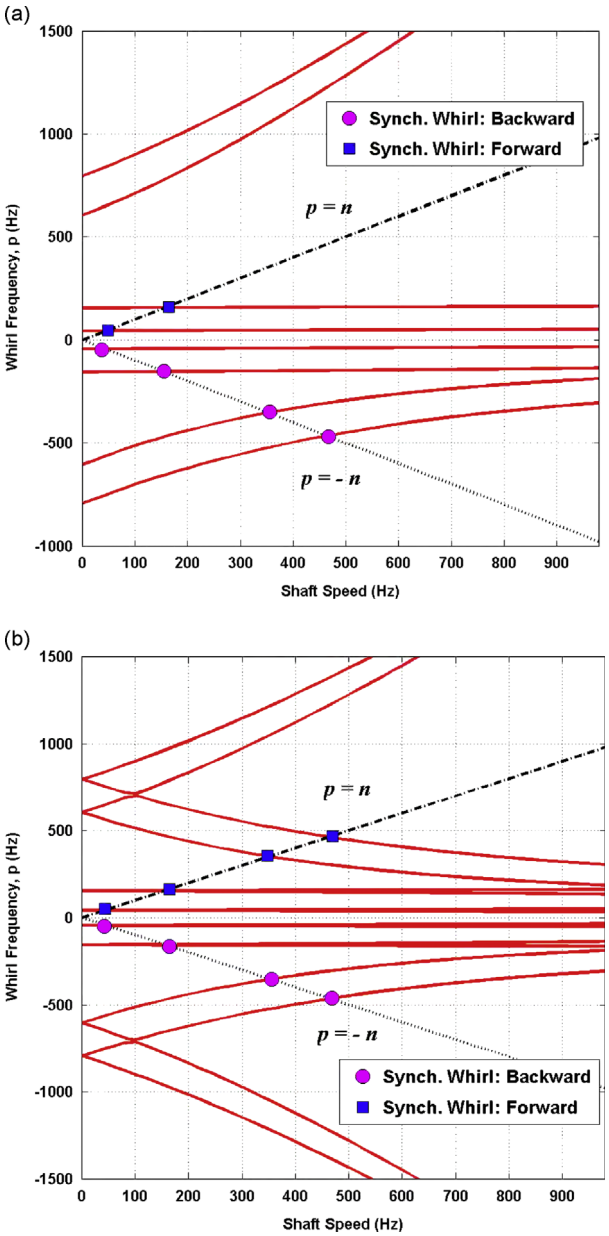

Fig. 6. Whirl frequency analysis of a rotor supported by elastomer rings. (a) CTM; (b) RTM.

Table 4
Natural frequencies.

	CTM	Scholz [33]	
	Analytic	Analytic	Experimental
$\omega_{n\,1}$	43.7 ($<1\%$)	43.8 (-0.4%)	43.7
$\omega_{n\,2}$	155.2 ($+4.5\%$)	153.2 ($+1.7\%$)	148.5

where the damping is incorporated by assuming a complex stiffness, $z(p)$, obtained from the viscoelastic correspondence principle:

$$z(p) = ND_m \pi k_L E'(p) + \mathrm{j}\, k(p)\eta(p) \tag{45}$$

The frequency-dependent storage and loss moduli are given by Eqs. (38) and (39). The CTM gives the bearing transfer matrix as

$$\mathbf{B} = \begin{bmatrix} 1 & 0 & 0 & 0 \\ 0 & 1 & 0 & 0 \\ 0 & 0 & 1 & 0 \\ -z(p) & 0 & 0 & 1 \end{bmatrix} \tag{46}$$

The frequency at which the elastomer is compressed is the frequency on which the stiffness and damping depend. In a rotordynamic free response, this frequency is the rotor's whirl frequency, p. The elegance of the correspondence principle coupled with the frequency-dependent constitutive model lies in the ability to directly obtain the whirl frequencies without any iteration or *a priori* assumption on the value of p appearing in Eqs. (38) and (39). The frequency-dependent stiffness and damping are included directly in the transfer matrix, and thus appear directly in the system's characteristic equation.

The overall transfer matrix in the inertial frame is

$$\mathbf{U} = \mathbf{B}\,\mathbf{F_3}\,\mathbf{P_2}\,\mathbf{F_2}\,\mathbf{P_1}\,\mathbf{F_1}\,\mathbf{B} \tag{47}$$

where each end of the shaft is supported by an identical elastomer ring. The previously discussed boundary conditions are applied to the overall transfer matrix to extract a submatrix, the determinant of which is the characteristic equation. The roots of this equation provide the whirl frequencies at each shaft speed, n. Since damping is included in the free response analysis, the eigenvalues are in actuality the damped eigenvalues.

5.3. Results

The Campbell diagram is found using the CTM and the RTM and shown in Fig. 6a and b, respectively. Application of the CTM resulted in approximately a five-fold decrease in required computation time, demonstrating an important advantage of the method. The forward and backward synchronous whirl frequencies are found by intersection between the locus of eigenvalues and lines of slope 1 and -1, respectively. Observing Figs. 6a and 6b, it is clear that the RTM fails to distinguish forward and backward whirl. Additional steps would be required to distinguish forward and backward whirl using the RTM, such as mode shape analysis, whereas whirl direction separation is intrinsic using the CTM.

The whirl frequencies corresponding to zero shaft rotation case are the natural frequencies of the beam in vibration. Table 4 compares the first and second natural frequencies predicted by the CTM to those given by Scholz [33], with percent differences relative to the experimental values. The analytic values given by Scholz [33] are generated using a finite element model accounting for the distributed nature of the shaft's mass. Interestingly, the values predicted are very close in magnitude to those of the simply supported rotor. Such an issue is foreseeable, as the stiffness of the elastomer rings is significantly greater than the stiffness of the shaft. However, the objective of the elastomer ring is not only to provide adequate stiffness, but also to reduce undesirable vibrations through exploitation of viscoelastic damping.

Several plausible explanations exist for the differences between the predictions. First, this work did not account for the actual distribution of mass along the shaft's length, but instead lumped a portion of the shaft's mass to the rotors. Higher modes are typically more sensitive to mass distribution; mass distribution approximations are likely to manifest in discrepancies between higher modes of vibration. This was indeed observed in the analysis, as the second natural frequency displayed a greater percentage error. A second source of possible error is incurred by fitting the experimental elastomer data to an analytic constitutive model. Accounting for a higher order approximation could perhaps reduce the order, at the cost of significantly complicating the analysis.

6. Conclusion

The Real Transfer Matrix (RTM) suffers from several notable deficiencies; namely, excessive computation time and the inability to distinguish forward and backward whirl. The Complex Transfer Matrix (CTM) is developed from the RTM using a

complex-valued coordinate redefinition of the state vector, reducing the dimension of the transfer matrices from 8×8 in the RTM to 4×4 in the CTM. Point and field matrices, including the effects of external stiffness and damping, are developed in the inertial and rotating reference frames. A brief discussion on the mathematical motivations for separation of whirl is provided, indicating that the RTM fails to distinguish backward and forward whirl due to the shaft speed appearing in the characteristic equation only in even powers. Two examples are provided to demonstrate the utility of the CTM and the transfer matrix in general. First, the whirl frequencies of a simple overhung rotor are found symbolically and numerically using the characteristic equation. Second, the whirl frequencies of a rotor supported on viscoelastic elastomer damping rings are found for the first time using the transfer matrix method. The transfer matrix method is very useful and particularly applicable for rotordynamic analysis, even when compared to finite element methods. As demonstrated, the transfer matrix method (and especially the CTM, due to the reduced dimension) is adept for symbolic manipulations. A second gainful attribute of the method is the ability to directly extract whirl frequencies and their direction without expenditure of significant computational resources.

The utility of the CTM is demonstrated by applying the method to obtain whirl frequencies of a rotor supported by viscoelastic elastomer ring damper supports. An expression for the frequency-dependent stiffness and damping of the elastomer ring is provided by fitting experimental data to a fractional calculus constitutive viscoelastic model. The frequency-dependent stiffness and damping are directly incorporated into the transfer matrix using the viscoelastic correspondence principle. The Campbell diagram is given using the RTM and the CTM, where the primary advantage of the CTM is noted: the intrinsic separation of forward and backward whirl. It is seen that the CTM provides results very close to those predicted analytically and experimentally by Scholz [33] and Liebich et al. [34].

The CTM can be further modified to include external harmonic forcing. Such a modification would permit investigation of the imbalance response (or response to any harmonic forcing) for rotordynamic systems. Second, the method described herein is valid only for shafts and bearings with isotropic stiffness. The method could be significantly enhanced by allowing for the inclusion of stiffness asymmetries such as fluid film bearings, asymmetric shafts, or cracked shafts.

Acknowledgments

This material is based upon work supported by the National Science Foundation under Grant no. 1100101.

References

[1] G. Genta, *Dynamics of Rotating Systems, Mechanical Engineering Series*, Springer Science and Business Media, Inc., New York, NY, 2005.
[2] J.S. Rao, *Rotor Dynamics*, 3 ed. New Age International, New Delhi, 1996.
[3] C.W. Lee, *Vibration Analysis of Rotors*, Kluwer Academic Publishers, Boston, 1993.
[4] J. Rao, Conditions for backward synchronous whirl of a flexible rotor in hydrodynamic bearings, *Mechanism and Machine Theory* 17 (1982) 143–152.
[5] A. Tondl, Some Problems of Rotor Dynamics, Publishing House of the Czechoslovak Academy of Sciences, 1965.
[6] P. Varney, Transverse Fatigue Crack Diagnosis in a Rotordynamic System Using Vibration Monitoring, Master's thesis, Georgia Institute of Technology, 2013.
[7] H. Nelson, J. McVaugh, The dynamics of rotor-bearing systems using finite elements, *Journal of Engineering for Industry* 98 (1976) 593–600.
[8] H.D. Nelson, A finite rotating shaft element using Timoshenko beam theory, *Journal of Mechanical Design* 102 (1980) 793–803.
[9] A. Darpe, K. Gupta, A. Chawla, Coupled bending, longitudinal, and torsional vibrations of a cracked rotor, *Journal of Sound and Vibration* 269 (2004) 33–60.
[10] N.O. Myklestad, A new method of calculating natural modes of uncoupled bending vibration of airplane wings and other types of beams, *Journal of Aeronautical Sciences* 11 (1944) 153–162.
[11] N.O. Myklestad, New method of calculating natural modes of coupled bending-torsion vibration of beams, *Transactions of the ASME* 67 (1945) 61–67.
[12] M. Prohl, A general method for calculating critical speeds of flexible rotors, *ASME Journal of Applied Mechanics* 67 (1945) 142–148.
[13] E. Pestel, F. Leckie, *Matrix Methods in Elastomechanics*, McGraw Hill, New York, New York, 1963.
[14] J. Lund, F. Orcutt, Calculations and experiments on the unbalance response of a flexible rotor, *Journal of Engineering for Industry* 89 (1967) 785–796.
[15] J. Lund, Stability and damped critical speeds of a flexible rotor in fluid-film bearings, *Journal of Engineering for Industry* 96 (1974) 509–517.
[16] B. Murphy, J. Vance, An improved method for calculating critical speeds and rotordynamic stability of turbomachinery, *Journal of Engineering for Power* 105 (1983) 591–595.
[17] A.S. Lee, I. Green, Rotordynamics of a mechanical face seal riding on a flexible shaft, *Journal of Tribology* 116 (1994) 345–351.
[18] S. Choi, S. Mau, Dynamic analysis of geared rotor-bearing systems by the transfer matrix method, *Journal of Mechanical Design* 123 (2001) 562–568.
[19] S. Hsieh, J. Chen, A. Lee, A modified transfer matrix method for the coupling lateral and torsional vibrations of symmetric rotor-bearing systems, *Journal of Sound and Vibration* 289 (2006) 294–333.
[20] S. Hsieh, J. Chen, A. Lee, A modified transfer matrix method for the coupled lateral and torsional vibrations of asymmetric rotor-bearing systems, *Journal of Sound and Vibration* 312 (2008) 563–571.
[21] Y. Kang, A. Lee, Y. Shih, Modified transfer matrix method for asymmetric rotor-bearing systems, *Journal of Vibrations and Acoustics* 116 (1994) 309–317.
[22] P. Varney, I. Green, Crack detection in a rotordynamic system by vibration monitoring. Part ii: extended analysis and experimental results, *Journal of Engineering for Gas Turbines and Power* 134 (2012). 112501.1–112501.10.
[23] P. Varney, I. Green, Rotordynamic crack diagnosis: *Distinguishing crack location and depth*, *Journal of Engineering for Gas Turbines and Power* 135 (2013). 112101.1–8.
[24] A. Liew, N. Feng, E. Hahn, On using the transfer matrix formulation for transient analysis of nonlinear rotor bearing systems, *International Journal of Rotating Machinery* 10 (2004) 425–431.
[25] J. Yu, On occurrence of reverse full annular rub, *ASME Journal of Engineering for Gas Turbines and Power* 134 (2012) 219–227.
[26] R.F. Beatty, Differentiating rotor response due to radial rubbing, *Journal of Vibration, Acoustics, Stress, and Reliability in Design* 107 (1985) 151–160.
[27] F.K. Choy, J. Padovan, Nonlinear transient analysis of rotor-casing rub events, *Journal of Sound and Vibration* 113 (1987) 529–545.
[28] J.J. Yu, P. Goldman, D.E. Bently, A. Muzynska, Rotor/seal experimental and analytical study on full annular rub, *ASME Journal of Engineering for Gas Turbines and Power* 124 (2002) 340–350.
[29] F. Dimentberg, Flexural Vibrations of Rotating Shafts, Butterworth's, London, 1961.

[30] R. Szumski, I. Green, Constitutive laws in time and frequency domains for linear viscoelastic materials, *Journal of the Acoustical Society of America* 90 (1991) 2292.
[31] P. Smyth, Viscoelastic Behavior of Articular Cartilage in Unconfined Compression, Master's Thesis, Georgia Institute of Technology, 2013.
[32] B.A. Miller, I. Green, Semi-analytical dynamic analysis of spiral-grooved mechanical gas face seals, *Journal of Tribology* 125 (2003) 403–413.
[33] A. Scholz, Ein Beitrag zur Optimierung des Schwingungsverhaltens Komplexer Rotorsysteme mit Viskoelastischen Dampfungselementen [A Contribution to the Optimization of the Vibration Behavior of Complex Rotor Systems with Viscoelastic Damping], Ph.D. Thesis, Technischen Universitat Berlin, 2011.
[34] R. Liebich, A. Scholz, M. Wieschalla, Rotors supported by elastomer-ring-dampings: experimental and numerical investigations, in: *10th International Conference on Vibrations in Rotating Machinery*, London.
[35] I. Green, C. Casey, Crack detection in a rotor dynamic system by vibration monitoring. Part I: *analysis*, *Journal of Engineering for Gas Turbines and Power* 127 (2005) 425–436.
[36] R. Gasch, Dynamic behavior of a simple rotor with a cross-sectional crack, in: Vibration in Rotating Machinery, IMechE.
[37] J.H. Ginsberg, *Mechanical and Structural Vibrations: Theory and Applications*, 1 ed. Wiley, New York, 2001.
[38] J. Snowdon, Rubberlike materials, their internal damping and role in vibration isolation, *Journal of Sound and Vibration* 2 (1964) 175–193.